Annals of Nuclear Energy 110 (2017) 36–47

Contents lists available at ScienceDirect

Annals of Nuclear Energy

journal homepage: www.elsevier.com/locate/anucene

CFD/Monte-Carlo neutron transport coupling scheme, application to TRIGA reactor

R. Henry [a,*], I. Tiselj [a], L. Snoj [b]

[a] Jožef Stefan Institute, Reactor Engineering Division R4, Jamova 39, SI-1000 Ljubljana, Slovenia
[b] Jožef Stefan Institute, Reactor Physics Division F8, Jamova 39, SI-1000 Ljubljana, Slovenia

ARTICLE INFO

Article history:
Received 14 February 2017
Received in revised form 6 June 2017
Accepted 12 June 2017
Available online 20 June 2017

Keywords:
Triga
Monte-Carlo
CFD
Coupling
Temperature measurement

ABSTRACT

A new computational model of the JSI TRIGA Mark II, coupling Monte Carlo neutron transport code TRIPOLI and fluid dynamics code CFX was built and verified with a set of new experimental data. A set of subroutines was developed to allow the communication between the Monte-Carlo transport code and CFD code. First, test of the coupling scheme is presented: for a given thermal power of the reactor, the coupled model numerically reproduced fuel temperature monitored during reactor operation and axial water temperature profile measured in the coolant channels. Then axial temperature profiles in the coolant channels were measured with a newly developed sensor during steady-state operation. Predictions of the coupled model are in expected agreement with experimental data recorded during reactor operations. Influence of the coupling has been investigated.

1. Introduction

Nuclear engineering is a complex crossover of several disciplines such as material science, chemistry, thermodynamics and particle physics. Each discipline describes the evolutions of physical quantities through set of mathematical equations. At the early days of nuclear engineering, slower computers required simplified models. Modelling assumptions were numerous (for example: one dimensional problem for thermal-hydraulics, point kinetic for neutronics...). Great improvement in computational power allows development of more accurate models able to describe interactions amongst nuclear, fluid, thermal chemical and structural behaviour of a nuclear reactor.

Multi-physics and multi-scale modelling is a particularly challenging task for the future (Ivanov and Avramova, 2007). More precisely, the coupled phenomena occurring in the core between neutronics and thermal-hydraulics are known as reactivity or thermal feedback. In water cooled reactor, thermal feedback and temperature coefficients of reactivity are important: a temperature variation impacts the neutron spectrum and the neutron flux profile. Those effects can have a significant impact on core's performance and inherent safety of the reactor.

Those reasons were naturally leading in the development of coupling methods in order to correctly predict the behaviour of the core in normal operation and accidental situation (Ivanov et al., 2013; Mylonakis et al., 2014; Zerkak et al., 2015). There are two ways to perform the coupling, the first one is called internal coupling in which all equations are solved simultaneously. Mahadevan (Mahadevan et al., 2012) have shown that this way of coupling provides better convergence, nevertheless, the number of equation to solve could be excessively large therefore several numerical challenges remain to be resolved. The coupling can also be external: a specialized code is used for each area of physics and the coupling is achieved with communication of the data between the codes (Vazquez et al., 2012). From an engineering point of view, this method allows the use of "state of the art" code thoughtfully verified and validated for each discipline. Downsides are the development of communication interfaces that are efficient on massive-parallel computer systems, accurate and stable (Kotlyar and Shwageraus, 2014). This last approach has been retained in the present paper.

The choice have been taken to couple a Monte-Carlo (MC) neutron transport code TRIPOLI (TRIPOLI-4 Project Team, 2013), with a computational fluid dynamic (CFD) code, Ansys CFX (ANSYS, 2011).

MC codes are gaining in popularity over deterministic codes, indeed, they enable the use of continuous nuclear data libraries and allow detailed modelling of complex geometry with minimum approximations (Wu and Kozlowski, 2015). Recently, MC codes were coupled with sub-channels code, MCNP5 and SUBCHANFLOW were used to predict the pin-power distribution of a PWR fuel assembly (Ivanov et al., 2013). Additionally, MCNP was coupled to various sub channel codes (Richard et al., 2015). SERPENT and DYNSUB were used to model a reactivity insertion accident

* Corresponding author.
E-mail address: romain.henry@ijs.si (R. Henry).

http://dx.doi.org/10.1016/j.anucene.2017.06.018
0306-4549/

(Knebel et al., 2016). Another example is the coupling between Serpent 2 and SUBCHANFLOW to simulate a full PWR under hot full power conditions (Daeubler et al., 2015).

Recently numerous coupling studies have been done with CFD and deterministic neutron transport codes to take advantage of their capabilities to reproduce 3 dimensional effects (Scheuerer et al., 2005). The coupling DeCART/STAR-CD was carried out to perform high fidelity simulations of boiling and pressurized water reactor (Weber et al., 2007). Ansys CFX and DYN3D were coupled to improve the steady-state description of PWR as well as few transient scenarios such as control rod insertion (Grahn et al., 2015).

Nevertheless, coupled studies based on MC and CFD are limited: both methods demand a lot of computational power. MCNP5/STAR-CD coupling was done to simulate a 3-D 3 by 3 array of PWR fuel pins (Seker et al., 2007). Another example are the coupled MCNP/Fluent simulations performed at University of Illinois to provide a high fidelity multi-physics simulation tools for analysis of the steady-state Pressurized Water Reactor core (Hu and Rizwan, 2008). More recently, steady-state of Pebble Bed-Advanced High Temperature reactor has been investigated with a coupled system RMC/CFX (Li et al., 2012). Super critical water reactor was also investigated with an external coupled system MCNP/CFX (Xi et al., 2013).

Fluid flow in the pool and in the core of the TRIGA reactor exhibits strong 3D features. For example, some of our simulations point to the possibility of internal recirculation inside the core: fluid is rising in the centre of the core and is flowing downward in some of the empty channels at the core periphery. This kind of phenomena justifies the implementation of the CFD approach. Another argument for using a CFD rather than subchannel codes for thermal-hydraulic analyses, is relatively simple geometry of the TRIGA reactor core. Roughly 40 cylindrical fuel elements and control rods can be relatively easily modelled with CFD. The same task is much more difficult in commercial reactors with several ten thousand fuel rods.

The purpose of this paper is to define a reference benchmark case for coupled thermal-hydraulic and neutronic calculations in a relatively simple geometry of the TRIGA reactor. The calculations are compared against the new experiments specially designed for the validation of the coupled model. After an overview of the TRIGA reactor, the thermal-hydraulic as well as the neutronic model are presented. The third part describes the coupling scheme. In order to validate the model a measurement campaign was performed to collect water temperature profile; presentation of the experimental protocol is given in the fourth part. Finally, the calculations are compared to the experiments to serve as a validation of the model.

2. TRIGA reactor

TRIGA® (Training Research Isotope General Atomics) is a pool-type nuclear research reactor manufactured by General Atomics. The reactor fuel is uranium zirconium hydride (U-ZrH) fuel. Fuel elements are cooled by demineralised water that flows through the reactor core by natural convection.

The TRIGA MARK II research reactor at the Jožef Stefan institute (JSI) is a typical 250 kW TRIGA reactor, which is used for various applications: such as neutron activation analysis, neutron radiography and tomography, education and training, radiation hardness studies and benchmark experiments for verification and validation of computer codes (Radulovic et al., 2014; Ravnik and Jeraj, 2003; Snoj et al., 2011; Žerovnik et al., 2015). During the long time reactor operation, an external cooling system is operating, which cools the upper section of the pool through a forced convection; however, natural convection remains the driving force for the flow through the core.

The core of TRIGA reactor is placed at the bottom of an open tank (atmospheric pressure) with 5 m of water column above it (Fig. 1). The core has a cylindrical configuration with 91 designed locations to accommodate fuel elements or other components such as control rods, a neutron source and irradiation channels. Elements are arranged in six concentric rings: A, B, C, D, E and F, each having 1, 6, 12, 18, 24 and 30 locations, respectively.

A graphite reflector enclosed in aluminium casing surrounds the core. An annular groove in the upper part of the reflector body is provided to contain a special irradiation facility. Detailed description (dimension, material composition...) of the reflector and every other component can be found in the paper of Ravnik and Jeraj (Ravnik and Jeraj, 2003).

The TRIGA reactor fuel is a homogeneous mixture of enriched uranium and zirconium hydride (U-ZrH) it is clad by stainless steel (SS304). The enrichment and content of uranium in U-ZrH depends on the fuel type (ICSBEP, 2013; Snoj and Ravnik, 2008) The main feature of such composition is that the fuel is homogenously mixed with moderator in the form of U-ZrH causing a large fraction of neutrons to be moderated in the fuel itself. Therefore one should pay special attention to the thermal scattering cross-sections, especially for H and Zr bound in ZrH as well as elastic scattering cross-sections for Zr (see discussion in Section 4.1, Step 4 of the algorithm) (Snoj et al., 2012).

3. Computational models

3.1. Neutron physics

The neutron transport simulations were performed with the Monte Carlo neutron transport code TRIPOLI. The geometry of the computational model is presented in Fig. 2. Fuel elements (red) and control rods (grey) are taken into account with full available precision, meaning that Zr rod, stainless steel cladding, air gaps and Mo supporting disc are explicitly resolved. The supporting grid, graphite reflector (in black) with rotary groove (cyan) and central irradiation channel (white) in the core are also explicitly resolved. Some elements cannot be seen in the picture but are modelled:

- irradiation channels in the core
- graphite of the thermalizing and thermal column
- carrousel with explicitly modelled irradiation tubes
- neutron source element
- triangular irradiation channel
- radial and tangential beam ports

The ENDF/B-VII.0 nuclear data set (Chadwick et al., 2006) was used for neutron transport calculations as well as for reaction rate calculations.

A more accurate description of the modelling assumption of the TRIPOLI model of TRIGA and its validation can be found in (Henry et al., 2015). The core configuration studied is very similar to the one used for reaction rates calculations of TRIGA Mark II reactor. The main difference being in control rod position and number of fuel rods and that the zero power condition is not imposed: temperatures of the fuel and water as well as the density of the water used in TRIPOLI are the one obtained from CFX.

3.2. Thermal-hydraulics

The CFD simulations were performed with the commercial code ANSYS® CFX. Two different models were used.

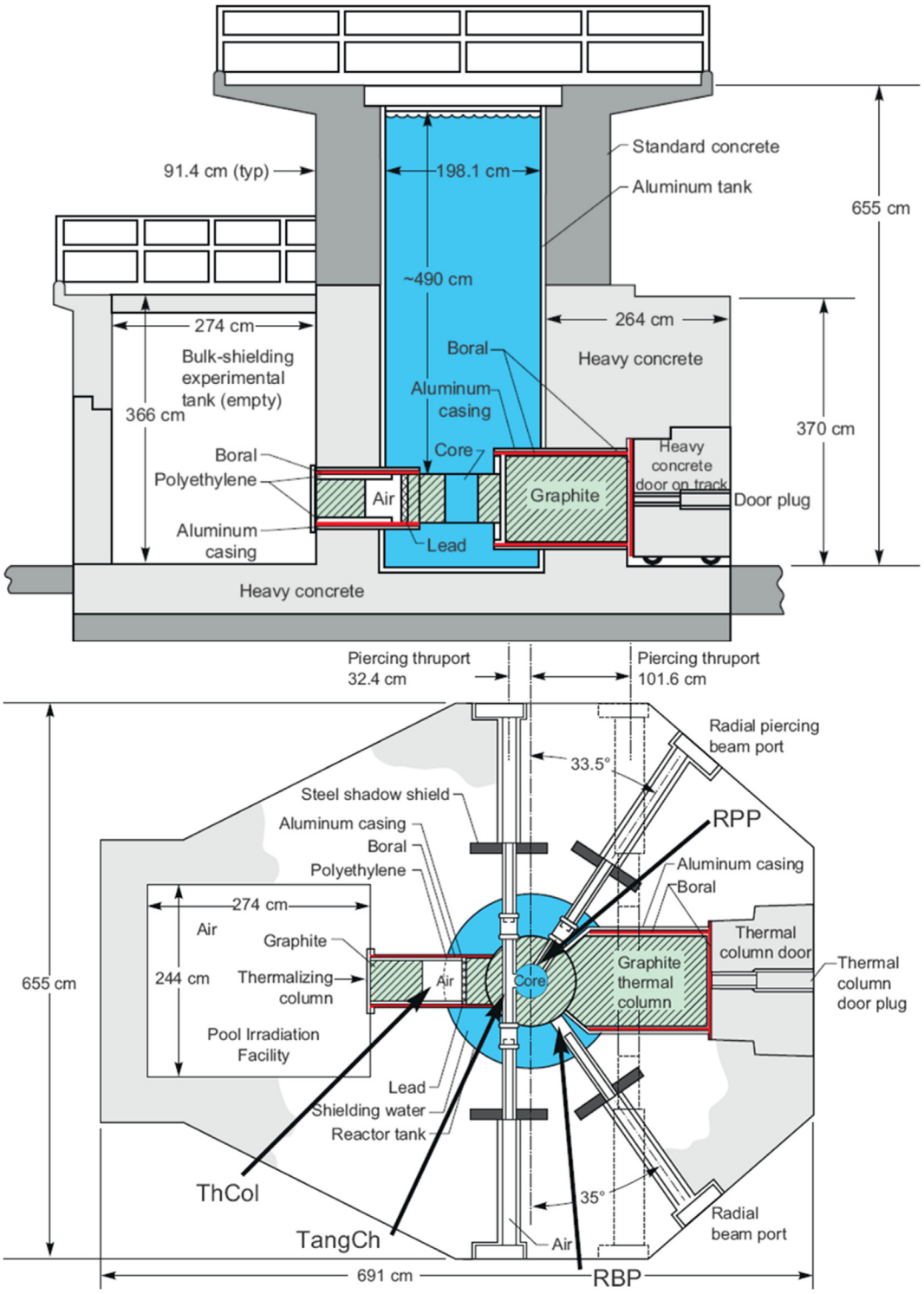

Fig. 1. Side and Top view of the JSI TRIGA Reactor (Ravnik and Jeraj, 2003).

First, the geometry of the entire pool, a 6.5 m high cylinder of diameter 2 m, was modelled. In this "full pool" model, the core was constituted of 58 fuel rods, 4 control rods and 5 irradiation channel of similar geometry (Fig. 3a). All these solid or air filled volumes were cut out from the computational domain. In the same way the volumes occupied by the graphite reflector and two thermal columns were cut out from the computational domain. Inlet and outlet pipes in the upper section of the pool were also modelled, although their pipes do not represent a significant obstruction for the flow. After few sensitivity analyses (geometry, mesh, turbulence model...), the model was validated with experimental results for two transients and for steady-state reactor operation (Henry et al., 2016).

In the present work, a new smaller and refined CFD model is used. The geometry considered is the domain confined inside the reflector (Fig. 3b). In this "core" model, fuel elements and control rods containing fuel part are fully modelled (rod, fuel, and cladding): a conjugate heat transfer problem is solved.

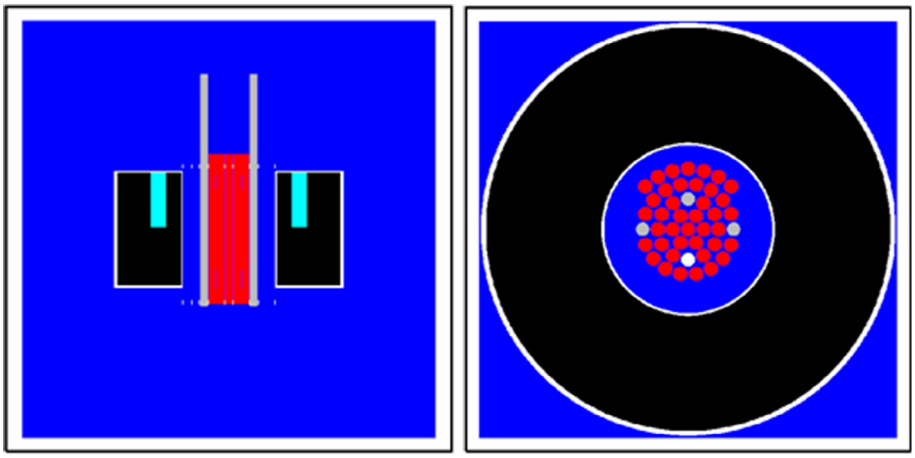

Fig. 2. Side and top view of the TRIPOLI Computational model.

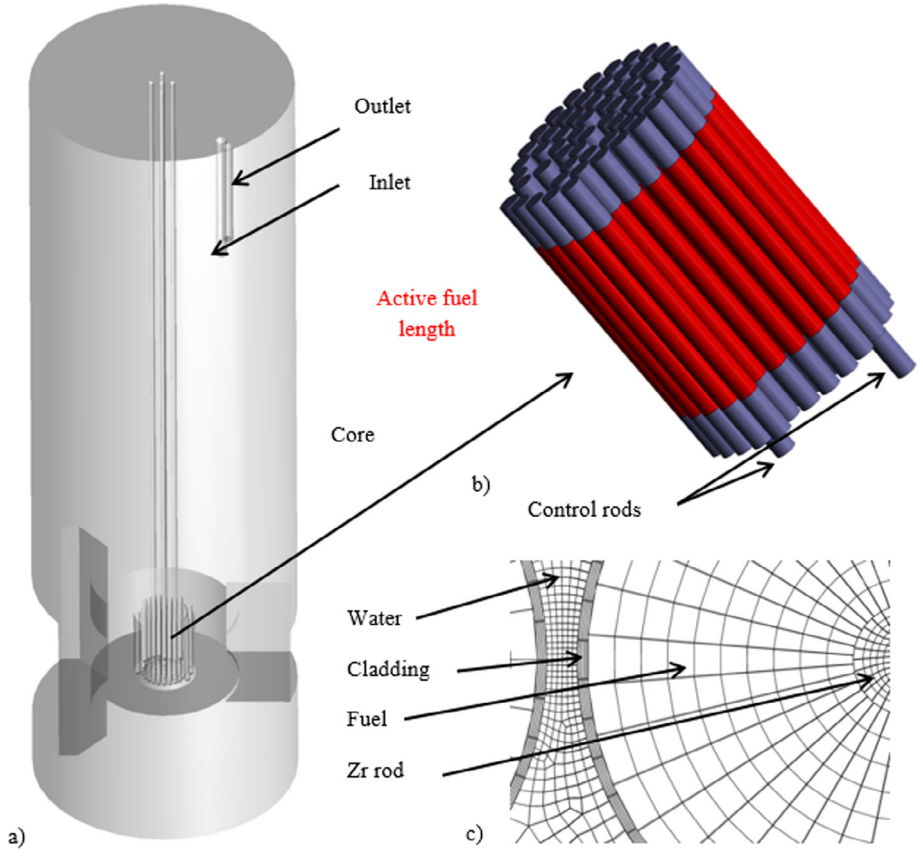

Fig. 3. "full pool" model (left) and "core" model (right up). Top view of the CFX mesh section of the "core" model. part of the fuel rod and coolant channel (approximately 2 cm × 1.5 cm) (right down).

At the inlet (bottom of the core) velocity distribution and temperature are imposed according to the steady-state converged solution of the "full pool" model. Different velocity distributions were calculated for various reactor powers. Pressure is specified at the outlet (top of the core). Power density distribution inside fuel elements was obtained from TRIPOLI calculation.

Buoyancy is the dominant heat transfer process (the Rayleigh number is about 10^{11}). Due to the non-negligible density variation inside the core, buoyancy is fully modelled in the Navier-Stokes equations.

Turbulence is described by the k-ε RANS model (Launder and Spalding, 1974). The impact of the turbulent model was studied for the "full pool" model (Henry et al., 2016).

Cross-section of a single fuel channel in the "core" model is shown in Fig. 3c. Each fuel part (38.1 cm high cylinder of radius 1.87 cm) is subdivided in $100 \times 10 \times 39$ elements (axial, radial and azimuthal respectively). Grid in the cooling channel is approximately $140 \times 20 \times 40$ (axial, radial and azimuthal respectively).

Water properties are function of the temperature (IAPWS tables). Solids thermal properties are summarised in Table 1.

Table 1
Thermal properties of the fuel rod components (Simnad, 1981).

Material	Cladding (SS)	Fuel (U-ZrH)	Rod (Zr)	Graphite (C)
Density (g/cm3)	7,89	6,04	6,49	1,6
Thermal conductivity (W/(m K))	17	22	23	80
Heat capacity (J/(kg K))	500	340	281	710

4. Coupling methodology

The steady-state conditions of a coupling neutronic/thermal-hydraulic problem can be deduced following this general data flow chart (Fig. 4). The code NJOY (MacFarlane et al., 2012) is a data processing system and can generate nuclear cross-sections at various temperature.

Detailed description of the coupled algorithm and how data are exchanged is presented in the following section.

4.1. Algorithm

The coupling scheme was developed between the Computational Fluid Dynamic (CFD) code ANSYS CFX and the Monte Carlo neutron transport code TRIPOLI. The coupling scheme was written following the recommendations of Dufek and Gudowski (Dufek and Gudowski, 2006) in order to ensure convergence and stability of the iterative process. Via the stochastic approximation, one can estimate the power density at iteration n, $p^{(n)}$, by:

$$p^{(n)} = (1-\alpha_n)p^{(n-1)} + \alpha_n p^{tripoli}(s_n, \sigma^{(n)}(T^{(n)}), \rho^{(n)}) \quad (1)$$

- α_n is a relaxation parameter (detailed below).
- s_n is the number of neutron histories to be simulated at iteration n. S_n is defined as the sum of the s_n.
- $\sigma^{(n)}$ are the cross-sections, dependant on the isotope and its temperature field $T^{(n)}$.
- $\rho^{(n)}$ is the coolant density.
- $p^{TRIPOLI}$ is the power density calculated by the TRIPOLI code.
- $\int\int\int p^{TRIPOLI}$ is the integral over space of the power density

Algorithm 1: Description of the coupling scheme.

1: Initialisation: Power P, s_0, $S_0 \leftarrow 0$
$p^{TRIPOLI} \leftarrow$ TRIPOLI($\sigma^{(0)}$ at $T^{(0)} = 300$ K, $\rho^{(0)} = 997$ kg m^{-3})
$p^{(0)} \leftarrow P * p^{TRIPOLI} / \int\int\int p^{TRIPOLI}$
For n = 1, 2 ... do
2: $s_n \leftarrow$ new value (method dependent)
$S_n \leftarrow s_{n-1} + s_n$
$\alpha_n \leftarrow s_n / S_n$
3: $T^{(n)}$, $\rho^{(n)} \leftarrow$ CFX($p^{(n-1)}$)
4: $\sigma^{(n)} \leftarrow$ NJOY($T^{(n)}$)
5: $p^{TRIPOLI} \leftarrow$ TRIPOLI($\sigma^{(n)}$, $\rho^{(n)}$)
6: $p^{(n)} \leftarrow (1-\alpha_n)\, p^{(n-1)} + \alpha_n\, P * p^{TRIPOLI} / \int\int\int p^{TRIPOLI}$
7: If (converged) STOP, else CONTINUE
End for

Here some steps of the algorithm are commented:

Step 1: The initial power density distribution is obtained with a criticality calculation at room temperature. The calculated distribution is normalised to obtain the desired thermal power P.

Step 3: In order to obtain the new temperature distribution (fuel and coolant) and the new density (coolant), the CFD code ANSYS CFX is executed in steady-state mode. In each iteration, the power distribution is updated with the value obtained at the previous iteration.

Step 4: Temperature distributions obtained at the previous step are a direct input to calculate temperature dependant microscopic cross-sections. The code NJOY is called via a new version of TRIPOLI allowing computation of the nuclear data at the requested temperature and post processing of the nuclear data at the format needed by TRIPOLI. Pseudo - material method (Conlin et al., 2005) is used for the S(a,b) tables.

Step 5: The power density distribution is evaluated by simulating s_n neutron histories with TRIPOLI in criticality mode. The fuel and coolant properties in the Monte Carlo neutron transport calculations are updated with the new cross-sections and density. It is important to note that the dimensions of the components are not changed.

Step 6: The relaxation is applied to the flux distribution.

The algorithm is stopped according to a criterion to be chosen. The common way to stop the simulation is to monitor the convergence of the relaxed solution:

$$\varepsilon = \alpha_n \| \varphi^{tripoli} - \varphi^{(n)} \|_\infty \quad (2)$$

When the absolute value of ε reached a certain value the algorithm is stopped.

The selection of the number of neutron histories, s_n, is directly impacting the relaxation parameter, α_n. One option is to fix s_n at a constant value. In that case α_n is generated according to the Robbins-Monro algorithm (Robbins and Monro, 1951):

$$\alpha_n = \frac{1}{n} \quad (3)$$

Dufek and Gudowski proposed an "optimal" way of varying s_n. Their idea is to let the number of neutron histories grow over the iteration steps in order to avoid wasting the computational time to calculate first flux iterations that might contain large errors. At every iteration s_n is deduced according to Eq. (4):

$$s_n = \frac{s_1 + \sqrt{s_1^2 + 4 s_1 S_{n-1}}}{2} \quad (4)$$

Every iteration, the number of neutron histories grows by adding around half of the first sample, s_1.

4.2. Data exchange

One challenge of the coupling is the communication of the variable of interest, in this case, temperature, density and power density (Fig. 4). Since the number of compositions in TRIPOLI is lower than the number of discrete volume in the CFX model, the definition of a suitable spatial mapping is very important. On one side, TRIPOLI needs a discrete set of temperatures, one for each composition. Consequently, an averaging operation is necessary on the CFX volume elements corresponding to this composition. On the other side, tallies from TRIPOLI are computed on a coarser mesh (each fuel element is subdivided in $10 \times 3 \times 3$ elements axial, radial and azimuthal respectively) than the CFD one. Interpolation is done to transmit the correct power density to each CFX volume element.

From the programing point of view, data transfer is handle through files. Fluid quantities are averaged and written in a file by the FORTRAN user routine developed for CFX. This file is then read by a shell script in order to update the input composition file of TRIPOLI. The calculated power density is read from the result file of TRIPOLI and modified (according to Algorithm 1) by the shell script before to be written in a file. The new power density is read and interpolated by the FORTRAN routine.

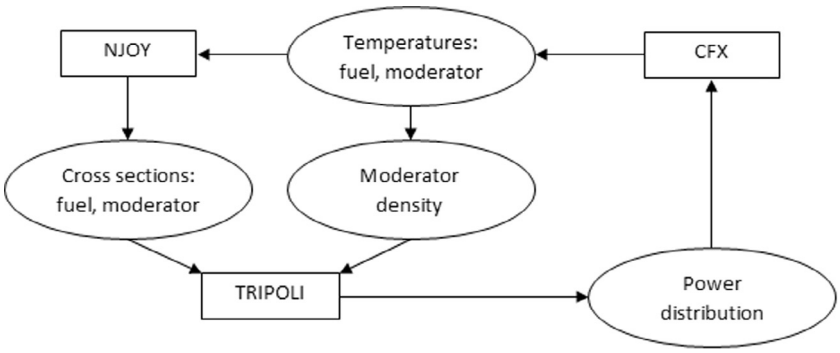

Fig. 4. Data flow chart during an iteration.

In the special case of the TRIGA reactor that is presented in Sect 6, temperature and density of the coolant have a minor effect on the power density. The TRIGA fuel made of uranium-zirconium hydride (U-ZrH) presents a homogenous mixture of fuel and moderator. Number density of H in U-ZrH (5.5 10^{22} atoms cm^{-3}) is very close to the number density of H in H2O (7.2 10^{22} atoms cm^{-3}), Hence significant part of moderation occurs already in the fuel. Consequently, temperature of the fuel has large effect on neutron spectrum changes. Since temperature variations for the fuel are significantly higher than for the water, a temperature for every fuel element should be considered while the average water temperature and density inside the domain was found to describe accurately the water from TRIPOLI point of view.

As a result of a sensitivity analysis described in Section 6.3.1, it was decided to use one "effective" temperature per fuel element. The "effective" temperature at which the neutron "see" the material was evaluated with the Rowlands formula (Rowlands, 1962):

$$T_{eff} = \frac{5}{9} T_{surface} + \frac{4}{9} T_{centre} \quad (5)$$

5. Experimental set-up

In order to measure water axial temperature profile in the core, ten temperature sensors have been positioned in the core as shown in Fig. 6. To minimize the amount of radioactive waste, K-type thermocouples made of nickel, chrome and aluminium were chosen. Indeed, these chemical elements have shorter decay time than coper, which is used in other type of thermocouples.

Furthermore, limited space available in the reactor core and the request for reduction of the radiation exposure during the experiments have dictated the construction of a guiding structure in aluminium, which, when activated, has a short decay half-time (2.3 min). It was custom built to perfectly fit into the measuring positions (MP) pierced into the top grid and to accommodate 10 thermocouples in a vertical column within the core (Fig. 5). Special attention was paid to: first, shield the temperature sensors from the hot surfaces of the fuel elements, second, keep the sensor's tips in contact with local coolant circulation.

Data acquisition application was developed in LabVIEW (National Instrument Corporation, 2003) running on Windows 7 platform to acquire temperature readings from the thermocouples and to perform the associated measurement statistics. PXI express chassis with integrated controller was used in combination with the NI (National Instrument Corporation, 2015) PXIe-4353 modules and the corresponding terminal blocks TB-4353 with powerful cold-junction compensation. The NI measurement hardware was calibrated to ensure that the device meets its published specifications. The main sources of experimental uncertainty are identified in the Table 2.

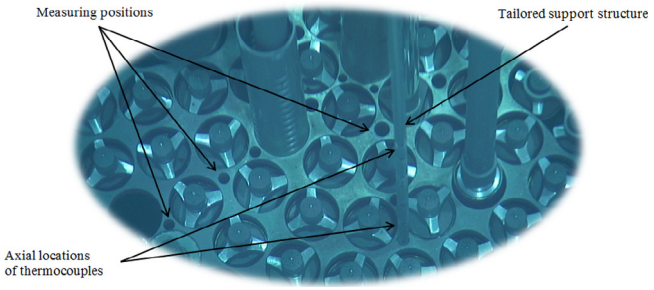

Fig. 5. Tailored support structure before insertion into a measuring position.

- Uncertainty on temperature is the typical accuracy of the NI PXIe-4353.
- Uncertainty on the radial position of the thermocouples is bounded by the radius of the guiding structure (4 mm).
- Uncertainty on the axial position of the thermocouples was estimated to be roughly the length (1 cm) of thermocouple facing the opening of the guiding structure.
- Uncertainty on the time measurement was estimated taking into account the time constant and the expected velocities of the coolant within the core, sample rate of 1 sample/s/channel was used.

The thermocouples were installed in the support structures and their readings were calibrated together with the acquisition system in a constant temperature reactor pool after several days of reactor non-operation: measurements of all 10 thermocouples were typically predicting the same temperature within a 0.2 °C dispersion band. The second source of uncertainty was spatial positioning of the support structure. On the other hand, accuracy of the time measurement was defined with the adjustable sample rate. In this context, taking.

Axial coolant temperature profiles along the narrow water column confined with hot fuel elements were acquired during steady-state operation. The support was inserted at different measuring positions (Fig. 6a). Axially thermocouples were spread between bottom and top grid such as describe in Fig. 6b. TCs are align, all the sensor are "looking" at the same direction. Different "orientations" are observed by rotating the structure inside a measuring position.

Temperature collected were post processed to allow comparison with the prediction of the CFX/TRIPOLI model.

6. Results and discussion

Coupled simulations were performed on a computer with 28 cores (two processors Intel(R) Xeon(R) CPU E5-2697 v3 at

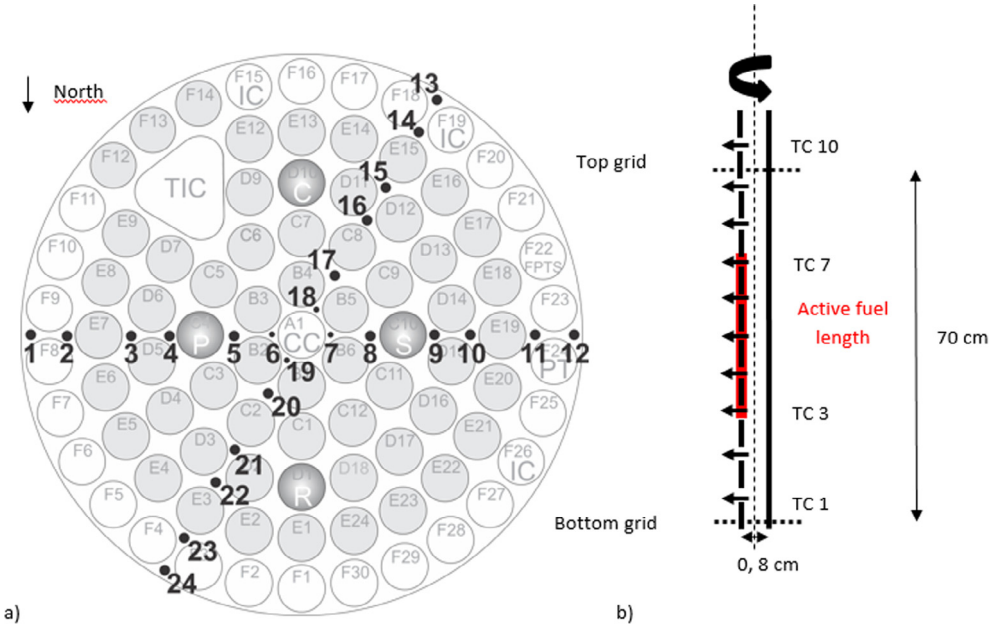

Fig. 6. Measuring positions in the core of the TRIGA reactor (left) and schematic of the axial position of the thermocouples (right).

Table 2
Experimental uncertainty of the temperature, position and time measurements.

T (°C)	δx (m)	δy (m)	δz (m)	δt (s)
±0.36	±0.004	±0.004	±0.01	±1

2.60 GHz of 14 cores) and 256 GB DDR4 memory. CFX uses five cores while TRIPOLI uses the totality. Convergence criterion for Eq. (3) was set to 0.1%. Final solution was reached within 11 iterations after 9 h, 80% of that time was used by TRIPOLI, 18% by CFX and less than 1% by NJOY. The computational time per iterative step grows linearly with the number of batches. Computation starts with 5000 batches of 1000 neutrons. Then the number of batches was increased according to Eq. (4). Statistical uncertainties of the neutronic scores were below 2%. Experimental and simulated results of steady-state operation are presented in the next section.

6.1. Demonstration case: 250 kW steady-state

Full power steady-state mode operation of the reactor was studied: the reactor is operated at constant power 250 kW. The heat produced is removed by the external cooling system; mixed convection is driving the flow. The pool is kept at an average temperature around 27 °C. Temperatures were recorded and averaged over a 5 min intervals, this time interval was found large enough to catch the bulk temperature (Fig. 7). Temperature oscillations are the consequences of the mixing between rising cold water and water heated by the fuel elements. In Fig. 7, the oscillations are higher at MP17 than MP10. This can be explained by the fact that the temperature recorded at MP17 is at position TC5 where the heat flux is higher than the one at position TC4.

Averaged value over the time with the corresponding average deviation are presented here after.

For every position, the structured was rotated by 90° to investigate various orientations. Temperature profiles observed inside the same channel were different (Fig. 8). The reference temperature is taken at the entrance of each channel, in order to observe the temperature elevation (referred as "Delta Temperature inlet").

Fig. 8 shows how the orientation of the TC can have a large influence on the temperature profile observed at a same position. For MP5, the presence of the transient rod (P in Fig. 6, control rod that features air follower and not fuel follower, in contrast to the other control rods. hence, there is no heating) in the neighbourhood causes a strong heterogeneity in term of heat sources. The mixing in this area results in large temperature gradients that our steady-state RANS turbulence model was able to observe. Nevertheless, it could not predict the characteristic time and length scales of the temperature oscillations above the core. Large scale oscillations could be captured with unsteady (URANS) turbulence modelling, which is foreseen in our future work.

Consequently, in the rest of the paper measured temperature refer to the averaged value over the 4 orientations (north, west, south and east) and are denoted EXP.

In order to present the most representative comparison between simulations and measurements, calculated temperatures were averaged. For each axial level, the domain considered for the averaging is an 8 mm circular cross-section of the cooling channel. Averaged profiles (denoted CFX ave) are presented. Additionally, the maximum (denoted CFX max) as well as the minimum (denoted CFX min) temperature inside each averaging surface are shown in Figs. 9 and 10.

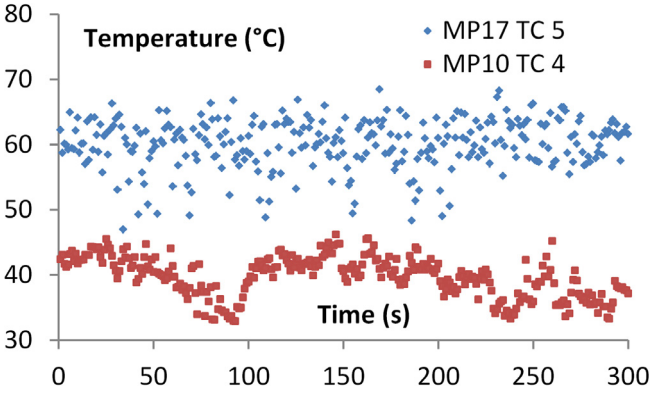

Fig. 7. Recorded measured temperatures by TC5 at MP17 and TC4 at MP10 (Fig. 6), both oriented toward the south, during typical 5 min interval.

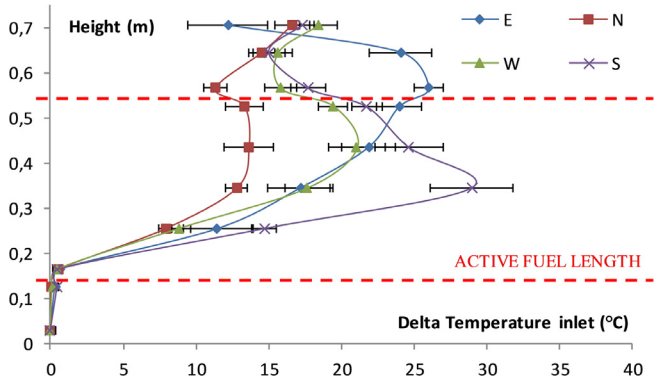

Fig. 8. Impact of the orientation of the TC on the temperature profile for the position MP5.

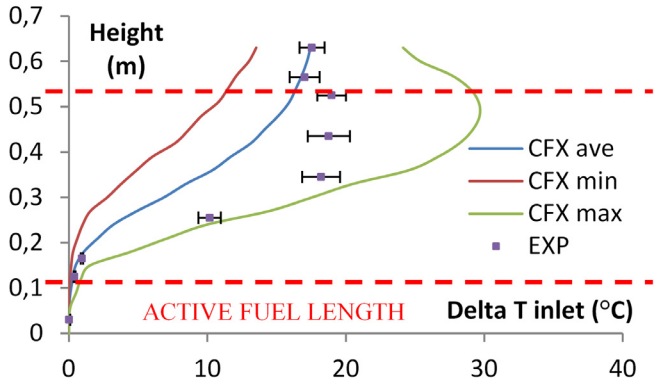

Fig. 9. Measured and calculated temperature axial profile at position 8.

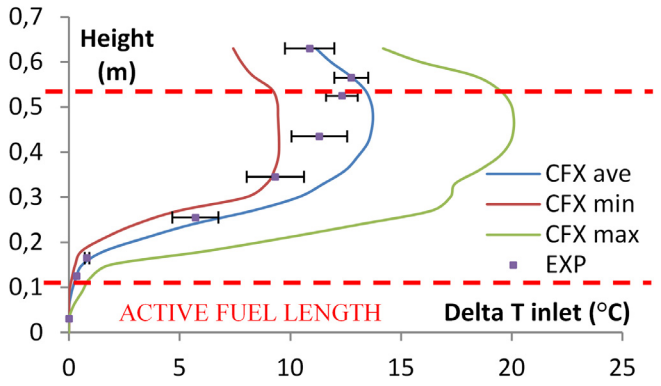

Fig. 10. Measured and calculated temperature axial profile at position 15.

All measuring positions were investigated but for the sake of clarity, the presentation is limited of axial temperature profiles for 2 positions: the worst (Fig. 9) and the best (Fig. 10) agreement between computations and measurements. Quantitative uncertainty analyse was not performed, however, visual checks of the measurement profiles did not show significant systematic bias.

For every position, measured values are framed by the minimum and the maximum CFX predictions. In general, most of the calculated profiles reproduced the shape observed during the measurements. And even for the few positions (MP18) where agreement of temperature profile inside the cooling channels was poor, the exit temperature was correctly predicted (Fig. 9). Discrepancies in the shape can be explained by the highly turbulent regime predicted by the high value of the Rayleigh number (10^{11}).

In Fig. 10, measured and simulated profiles are in very good agreement. Indeed, the maximum difference observed is 2 °C, while the average deviation is around 1 °C.

In general it was observed that the axial temperature gradient under the active fuel length is quasi null. Nevertheless small deviations could be observed in the neighbouring position of inserted control rods (positions R and S in Fig. 6). The explanation is simple; these two control rods contain active bottom part loaded with fuel length (so called fuelled follower) and perturb the temperature distribution.

Above this level the water temperature starts to increase as well as the amplitude of its oscillations. It was observed that the axial temperature gradient started decreasing a bit above the mid-plane of the core (TC5 in Fig. 5) and became negative, indicating the beginning of the mixing, a bit under the top grid.

Figs. 11and 12 present the temperature differences along the length of the cooling channels (between positions TC10 and TC1). For experiment temperature values are plotted with the average deviation associated. For calculation values are plotted with the maximum and the minimum temperature difference (between positions TC10 and TC1) predicted inside each cooling channel.

Except for MP16, measured values are in the range predicted by the coupled model. The maximum differences observed are for MP16 and MP17 where the model predicts for about 4 °C higher exit temperatures. This result gives strong reliability to the coupled model to predict accurately the temperature field as well as the velocity field. Figs. 13 and 14 show the average velocity at the exit of the different cooling channel. As it was expected, velocities are higher in the centre of the core than at the periphery. Velocity range varies from 0 up to 20 cm s^{-1}, for comparison the

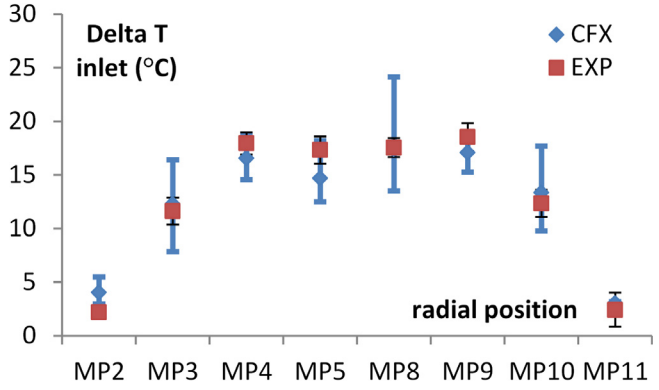

Fig. 11. Temperature differences along the length of the cooling channel MP2 to MP11.

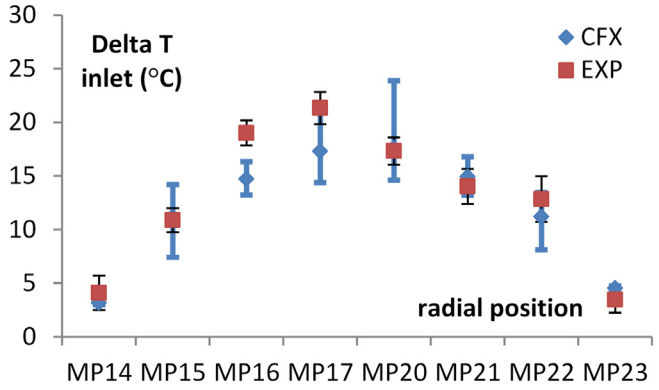

Fig. 12. Temperature differences along the length of the cooling channel MP14 to MP23.

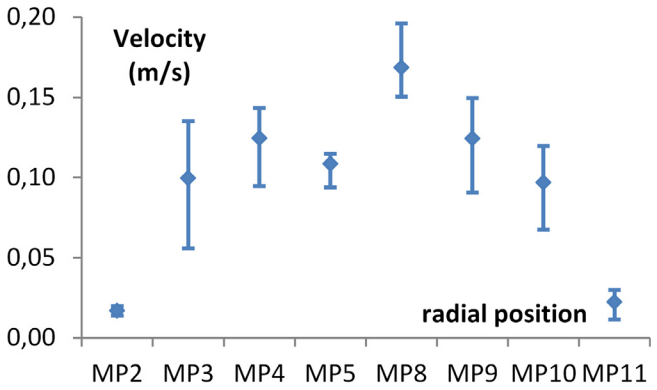

Fig. 13. Calculated axial velocity of the cooling channel MP2 to MP11.

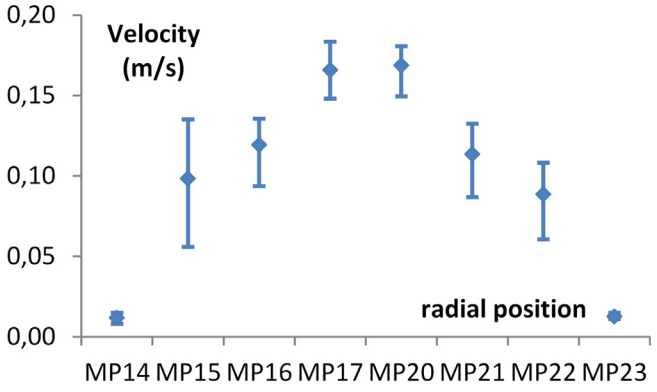

Fig. 14. Calculated axial velocity of the cooling channel MP14 to MP23.

recommended value by the manufacturer is 10 cm s^{-1}. Distribution seems quite symmetric except for MP5, the presence of the transient rod explains the velocity value lower than the one expected for a measuring position between B and C rings.

This distribution could become particularly handy for anyone wishing to evaluate the transport of radioactive elements inside the reactor core.

6.2. Impact of the coupling

Differences between the coupled model predictions and an uncoupled solution have been investigated. For this, the power density has been calculated by TRIPOLI with fuel isotopes at room temperature (294 K). Temperatures of the coupled model computed with the Rowland formula (Eq. 6) are higher. Therefore, due to the negative temperature feedback of the U ZrH fuel, the neutron flux calculated by Monte-Carlo method is in absolute value reduced element by element. Since the flux is then renormalized in order to achieve the expected same power level (250 kW), a redistribution of the power from the hottest elements (as B1) to the coolest elements (as E22) is observed numerically as shown in Fig. 15.

This result also assesses the ability of the model to describe correctly the expected fuel temperature feedback effects and shows how thermal-hydraulics impact neutronics.

The power densities were then used by CFX to calculate the temperatures field. Figs. 16and 17 show how the redistribution of the power slightly impacts the water temperature, strongest effect is observed at mid-plan (TC5 in Fig. 6). The coupled model

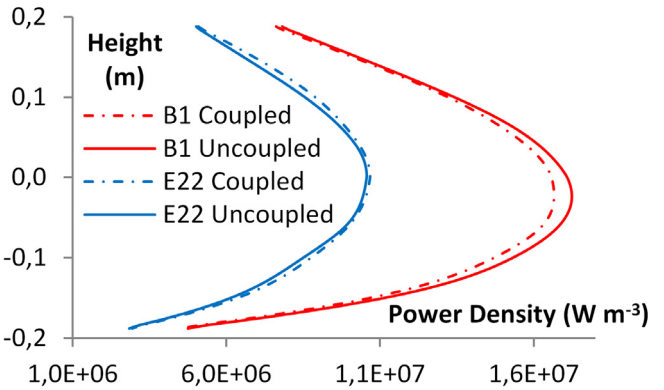

Fig. 15. Axial Power density calculated for fuel element B1 and E22 for different effective fuel temperature.

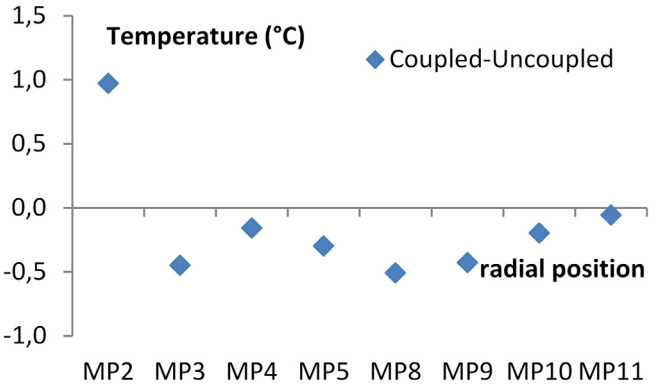

Fig. 16. Temperature difference between coupled and uncoupled solutions for the cooling channel MP2 to MP11 at position TC5.

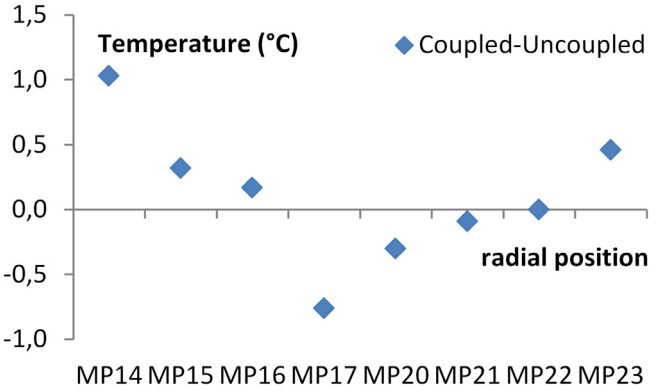

Fig. 17. Temperature difference between coupled and uncoupled solutions for the cooling channel MP14 to MP23 at position TC5.

predicts higher (resp. lower) temperature at the periphery (resp. centre) of the core.

This result shows how the neutronics impact the thermal-hydraulics.

Even if effects are smalls, the coupled model has shown how each discipline impact the other. Nevertheless, it is not possible to affirm that the coupled model described more accurately the physics of the TRIGA reactor despite the data collected during the experimental campaign.

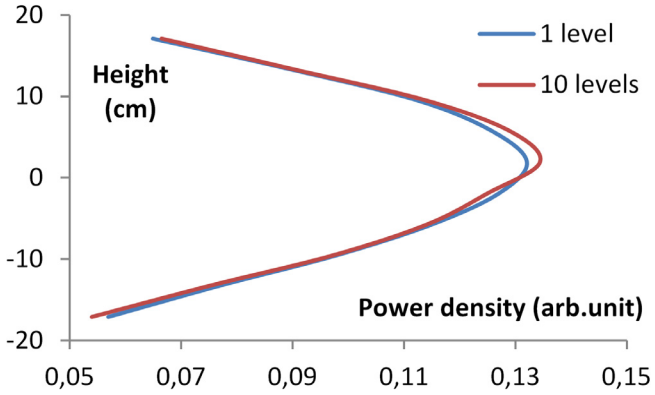

Fig. 18. Axial power density profile in a fuel element.

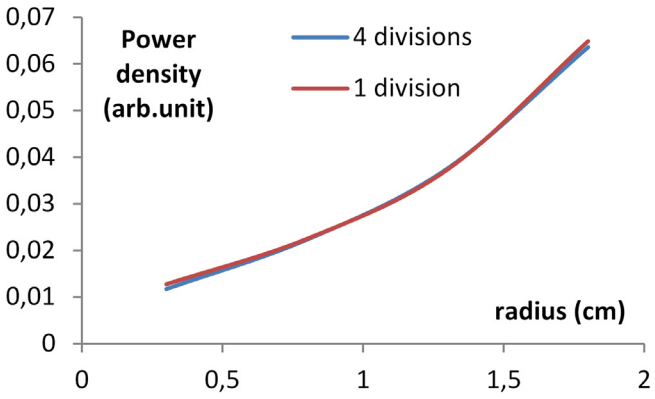

Fig. 19. Radial power density profile in a fuel element at mid plane.

6.3. Sensitivity analysis

In order to justify the modelling assumptions, different analysis were carried out:

- Effective fuel temperature definition.
- Influence of the gap conductivity.
- Measuring structure influence.

6.3.1. Effective fuel temperature

For simulations of TRIGA, the choice of assigning one temperature by fuel element for computation of cross-sections with NJOY was done. Beforehand, the effect of different temperature for different axial and radial region in one fuel element was studied. To do so, a single fuel element surrounded by water was modelled. In one case, the fuel part was subdivided in 10 axial levels and in 4 radial divisions. Each region had a different temperature. On the other case the same "effective" temperature was affected to each region. This temperature was computed from the Rowlands formula (Eq. 6).

Figs. 18 and 19 show the power density predicted in both cases. The total power was normalised to 1.

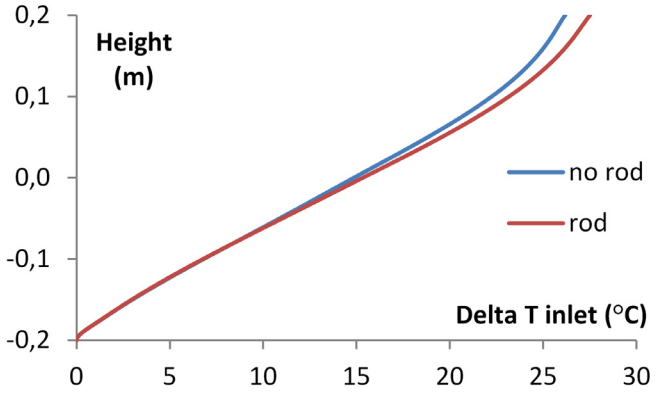

Fig. 20. Calculated temperature difference profile along the cooling channel.

Radially (Fig. 19), the impact is insignificant. Axially (Fig. 18), the use of only one temperature slightly underestimates the power density at mid plane and overestimates it at the top of the fuel. Nevertheless, relative differences between the two profiles stay below 3 %. Computational time was also 1 5% longer for this simple model with the subdivision of the fuel. Therefore the need to model it did not seem necessary.

6.3.2. Gap thermal conductivity

A sensitivity analysis, on the fuel temperature, was performed to conclude that the thermal contact resistance between the cladding and the fuel is negligible. Two fuel elements, B1 and C10 (Fig. 6) are equipped with 3 thermocouples located in the centre of the rod. The first one is at half length of the fuel element, the second (resp. third) is 1, 5 cm above (resp. below) the first one. Table 3 sums up the value obtained during reactor operation for 2 power levels and the temperatures predicted by the model.

For measured values, the 3 monitored values (1st, 2nd, and 3rd) are available for each element. Values were recorded during 10 min during steady-state operations at 50 and 250 kW. Since the radial positions of the TCs are not precisely known, the interval of temperature at half length of the fuel element is presented for calculated values.

The non-zero thermal resistance is the recommended value by the manufacturer (Mesquita and Gomes do Prado Souza, 2014) for fresh fuel element. The zero value corresponds to the conclusion of the sensitivity analysis in order to approach the real state of the reactor fuel temperature, since to the best of our knowledge no data about the effective thermal resistance are known.

6.3.3. Measuring structure influence

Results in the previous section were obtained with a model that did not take into account the TCs support. A small model of a cooling channel of TRIGA was considered to determine if the structure represent a significant additional hydraulic friction for the flow. Two geometries were considered, one with the measuring rod and one without denoted respectively "rod" and "no rod" in Fig. 20. In both cases the inlet velocity was imposed (5 cm s^{-1}).

Table 3
Simulated and measured fuel temperature for steady-state conditions.

Power (kW)	T measured (°C)		T calculated (°C)			
	B1	C8	Rth = 0 m^2 K W^{-1}		Rth = 4 10–4 m^2 K W^{-1}	
			B1	C8	B1	C8
50	(89;88;86)	(86;86;83)	[74:88]	[74:87]	[88:100]	[88:98]
250	(237;228;232)	(230;237;222)	[205:245]	[220:255]	[270:310]	[290:321]

Fig. 20 presents the temperature difference profile along the cooling channel predicted by the channel model with and without measuring rod. The maximum absolute difference occurs at the top of the channel and is smaller than 2 °C. This discrepancy should be compared with the deviation between maximum and minimum temperature prediction observed in Fig. 9 and Fig. 10. This temperature difference can be up to 20 °C. Finally, the need to model the rod did not appear to be of prime importance.

7. Conclusions

A computational fluid dynamic model of the reactor core was built. Conjugate heat transfer between solids (fuel, cladding, zirconium rod and graphite) and fluid part was modelled. This model was coupled with the TRIPOLI Monte Carlo neutron transport code. The coupling scheme was tested successfully on the steady-state operation of the JSI TRIGA reactor.

An experimental campaign aiming to study the temperature profiles of the coolant inside the core was performed. Measurements revealed that a lot of mixing occurs among the fuel rods since very different profiles can be observed at the same position just by rotating the measuring device.

Prediction of the coupled model and measurements were compared. In general good agreement was obtained while comparing axial temperature profile at every measuring position. Furthermore calculations reproduce accurately temperature radial profile at the exit of the core. This particular result gives good reliability to the model to predict the velocity inside the core. Various sensitivity analyses have been performed to ensure the reliability of the simulations, as the most representative modelling assumptions have been chosen.

Influence of the coupling has been investigated. Whereas the effects are smalls, the negative fuel temperature feedback has been observed with the power redistribution imposed by the temperature of the fuel.

Transient upgrade of the scheme is foreseen. The main difference for transient problems lies on the need of data exchange at every time step between the different codes. Another difficulty is the adaptation of Monte Carlo calculation to transient problem. One way investigated is to consider an adiabatic approximation and to split the neutron flux as the product of a function of space and energy (given by a Monte Carlo calculation) and a function of time that describes the fast variation of the flux and can be resolved by the kinetic equation.

Acknowledgments

The authors gratefully acknowledge the valuable contributions of our colleague Marko Matkovič and the reactor operator staff at JSI. In particular, Anže Jazbec, Darko Kavšek, Sebastjan Rupnik and Marko Rosman, for their help from the conception to the realization of the experiment. Research was founded by P2-0026 research program Nuclear engineering.

References

Ansys, I., 2011. User's Guide, ANSYS 14.0 Documentation.
Chadwick, M.B., Obložinský, P., Herman, M., Greene, N.M., McKnight, R.D., Smith, D. L., Young, P.G., MacFarlane, R.E., Hale, G.M., Frankle, S.C., Kahler, A.C., Kawano, T., Little, R.C., Madland, D.G., Moller, P., Mosteller, R.D., Page, P.R., Talou, P., Trellue, H., White, M.C., Wilson, W.B., Arcilla, R., Dunford, C.L., Mughabghab, S.F., Pritychenko, B., Rochman, D., Sonzogni, A.A., Lubitz, C.R., Trumbull, T.H., Weinman, J.P., Brown, D.A., Cullen, D.E., Heinrichs, D.P., McNabb, D.P., Derrien, H., Dunn, M.E., Larson, N.M., Leal, L.C., Carlson, A.D., Block, R.C., Briggs, J.B., Cheng, E.T., Huria, H.C., Zerkle, M.L., Kozier, K.S., Courcelle, A., Pronyaev, V., van der Marck, S.C., 2006. ENDF/B-VII.0: next generation evaluated nuclear data library for nuclear science and technology. Nucl. Data Sheets 107, 2931–3060.
Conlin, J.L., Ji, W., Lee, J.C., Martin, W.R., 2005. Pseudo material construct for coupled neutronlc-thermal-hydraulic analysis of VHTGR. Trans. Am. Nucl. Soc., 225–227
Daeubler, M., Ivanov, A., Sjenitzer, B.L., Sanchez, V., Stieglitz, R., Macian-Juan, R., 2015. High-fidelity coupled Monte Carlo neutron transport and thermal-hydraulic simulations using Serpent 2/SUBCHANFLOW. Ann. Nucl. Energy 83, 352–375.
Dufek, J., Gudowski, W., 2006. Stochastic approximation for Monte Carlo calculation of steady-state conditions in thermal reactors. Nucl. Sci Eng. 152, 274–283.
Grahn, A., Kliem, S., Rohde, U., 2015. Coupling of the 3D neutron kinetic core model DYN3D with the CFD software ANSYS-CFX. Ann. Nucl. Energy 84, 197–203.
Henry, R., Tiselj, I., Matkovič, M., 2016. Natural and mixed convection in the cylindrical pool of TRIGA reactor. Heat Mass Transf., 1–15
Henry, R., Tiselj, I., Snoj, L., 2015. Analysis of JSI TRIGA MARK II reactor physical parameters calculated with TRIPOLI and MCNP. Applied radiation and isotopes : including data, instrumentation and methods for use in agriculture, industry and medicine. 97, 140–148.
Hu, J., Rizwan, u., 2008. Coupled neutronics and thermal-hydraulics simulations using MCNP and FLUENT. Trans. Am. Nucl. Soc., 606–608
ICSBEP, 2013. International Handbook of Evaluated Critical Safety Benchmark Experiments, Paris.
Ivanov, A., Sanchez, V., Stieglitz, R., Ivanov, K., 2013. High fidelity simulation of conventional and innovative LWR with the coupled Monte-Carlo thermal-hydraulic system MCNP-SUBCHANFLOW. Nucl. Eng. Des. 262, 264–275.
Ivanov, K., Avramova, M., 2007. Challenges in coupled thermal-hydraulics and neutronics simulations for LWR safety analysis. Ann. Nucl. Energy 34, 501–513.
Knebel, M., Mercatali, L., Sanchez, V., Stieglitz, R., Macian-Juan, R., 2016. Validation of the Serpent 2-DYNSUB code sequence using the Special Power Excursion Reactor Test III (SPERT III). Ann. Nucl. Energy 91, 79–91.
Kotlyar, D., Shwageraus, E., 2014. Numerically stable Monte Carlo-burnup-thermal hydraulic coupling schemes. Ann. Nucl. Energy 63, 371–381.
Launder, B.E., Spalding, D.B., 1974. The numerical computation of turbulent flows. Comput. Methods Appl. Mech. Eng. 3, 269–289.
Li, L.S., Yuan, H.M., Wang, K., 2012. Coupling of RMC and CFX for analysis of pebble bed-advanced high temperature reactor core. Nucl. Eng. Des. 250, 385–391.
MacFarlane, R.E., Muir, D.W., M Boicourt, R., Kahler, A.C., 2012. The NJOY Nuclear Data Processing System, Version 2012.
Mahadevan, V.S., Ragusa, J.C., Mousseau, V.A., 2012. A verification exercise in multiphysics simulations for coupled reactor physics calculations. Prog. Nucl. Energy 55, 12–32.
Mesquita, A.Z., Gomes do Prado Souza, R.M., 2014. Thermal-hydraulic and neutronic experimental research in the TRIGA reactor of Brazil. Prog. Nucl. Energy 76, 183–190.
Mylonakis, A.G., Varvayanni, M., Catsaros, N., Savva, P., Grigoriadis, D.G.E., 2014. Multi-physics and multi-scale methods used in nuclear reactor analysis. Ann. Nucl. Energy 72, 104–119.
National Instrument Corporation, 2003. LabVIEW™User Manual.
National Instrument Corporation, 2015.
Radulovic, V., Stancar, Z., Snoj, L., Trkov, A., 2014. Validation of absolute axial neutron flux distribution calculations with MCNP with 197Au(n, gamma)198Au reaction rate distribution measurements at the JSI TRIGA Mark II reactor. Appl. Radiat. Isot. Incl. Data Instrum. Methods Use Agric. Ind. Med. 84, 57–65.
Ravnik, M., Jeraj, R., 2003. Research reactor benchmarks. Nucl. Sci. Eng. 145, 145–152.
Richard, J., Galloway, J., Fensin, M., Trellue, H., 2015. SMITHERS: an object-oriented modular mapping methodology for MCNP-based neutronic–thermal hydraulic multiphysics. Ann. Nucl. Energy 81, 150–163.
Robbins, H., Monro, S., 1951. Stochastic approximation method. Ann. Math. Stat. 22, 400–407.
Rowlands, G., 1962. Resonance absorption and non-uniform temperature distributions. J. Nucl. Eng. Parts A/B. 16, 235–236.
Scheuerer, M., Heitsch, M., Menter, F., Egorov, Y., Toth, I., Bestion, D., Pigny, S., Paillere, H., Martin, A., Boucker, M., Krepper, E., Willemsen, S., Muhlbauer, P., Andreani, M., Smith, B., Karlsson, R., Henriksson, M., Hemstrom, B., Karppinen, I., Kimber, G., 2005. Evaluation of computational fluid dynamic methods for reactor safety analysis (ECORA). Nucl. Eng. Des. 235, 359–368.
Seker, V., Thomas, J.W., Downar, T.J., 2007. Reactor physics simulations with coupled Monte Carlo calculation and computational fluid dynamics. In: Proceedings of the 2007 International Conference on Emerging Nuclear Energy Systems (ICENES-2007).
Simnad, M.T., 1981. The U-ZrHx alloy: its properties and use in TRIGA fuel. Nucl. Eng. Des. 64, 403–422.
Snoj, L., Kromar, M., Zerovnik, G., Ravnik, M., 2011. Advanced methods in teaching reactor physics. Nucl. Eng. Des. 241, 1008–1012.
Snoj, L., Ravnik, M., 2008. Power peakings in mixed TRIGA cores. Nucl. Eng. Des. 238, 2473–2479.
Snoj, L., Trkov, A., Ravnik, M., Žerovnik, G., 2012. Testing of cross section libraries on zirconium benchmarks. Ann. Nucl. Energy 42, 71–79.
TRIPOLI-4 Project Team, 2013. TRIPOLI-4 Version 8 User Guide.
Vazquez, M., Tsige-Tamirat, H., Ammirabile, L., Martin-Fuertes, F., 2012. Coupled neutronics thermal-hydraulics analysis using Monte Carlo and sub-channel codes. Nucl. Eng. Des. 250, 403–411.
Weber, D.P., Sofu, T., Won, S.Y., Downar, T.J., Thomas, J.W., Zhong, Z., Cho, J.Y., Kim, K.S., Chun, T.H., Joo, H.G., Kim, C.H., 2007. High-fidelity light water reactor analysis with the numerical nuclear reactor. Nucl. Sci. Eng. 155, 395–408.

Wu, X., Kozlowski, T., 2015. Coupling of system thermal-hydraulics and Monte-Carlo code: convergence criteria and quantification of correlation between statistical uncertainty and coupled error. Ann. Nucl. Energy 75, 377–387.
Xi, X., Xiao, Z.J., Yan, X., Li, Y.L., Huang, Y.P., 2013. The axial power distribution validation of the SCWR fuel assembly with coupled neutronics-thermal hydraulics method. Nucl. Eng. Des. 258, 157–163.
Zerkak, O., Kozlowski, T., Gajev, I., 2015. Review of multi-physics temporal coupling methods for analysis of nuclear reactors. Ann. Nucl. Energy 84, 225–233.
Žerovnik, G., Kaiba, T., Radulović, V., Jazbec, A., Rupnik, S., Barbot, L., Fourmentel, D., Snoj, L., 2015. Validation of the neutron and gamma fields in the JSI TRIGA reactor using in-core fission and ionization chambers. Appl. Radiat. Isot. 96, 27–35.